that the photoreaction is strongly inhibited in the en complex and that nonradiative decay to the ground state is a more effective competitor.

Part of this rate inhibition in the en complex could arise prior to reverse intersystem crossing because the larger energy barrier for the activated route allows more competitive doublet nonradiative decay. However, the extent to which such decay can be accommodated is restricted by the observed linearity of the Arrhenius plot. At the transition-state level, other possible reasons are easy to imagine. If the transition state is seven-coordinate, then it may be more sterically crowded and have higher strain energy for the en complex than for the diammine. Alternatively, it may be that the required migration of the whole en ligand is a difficult and slow process so that deactivation and/or recoordination have a greater opportunity to compete.

Finally, the diammine complex reacts[27] via a seven-coordinate species of microsecond lifetime. If the en complex behaves similarly, then its intermediate might be more likely to revert to starting material because of the bidentate nature of the leaving ligand.

Concluding Remarks. We have presented evidence that after photochemical Cr–N bond breaking has occurred, it is possible for the reacting bidentate ligand to migrate from one coordination site to another in an edge displacement reaction. Since our proof relies on the assumption of stereochemical change, in the future additional evidence will be sought. It is fairly straightforward to design experiments with appropriate stereochemical sign-posting to prove group migration incontrovertably. Unfortunately, it is difficult to identify systems in which the starting compound can be prepared and unambiguously characterized and its photochemistry explored with product identification including stereochemistry. The work has shown, however, that complex ligand motions are likely and that further study of such phenomena is tractable and worth pursuing.

Acknowledgment. We are grateful to the Natural Sciences and Engineering Research Council and the University of Victoria for financial support.

Contribution from the Institute of Chemistry, Academia Sinica, Nankang, Taipei, Taiwan (ROC)

Electron Transfer in Mixed-Valence Biferrocenium Salts: Effect of Zero-Point Energy Difference and Pronounced Anion Dependence

Teng-Yuan Dong,* Chi-Chang Schei, Tsui-Ling Hsu, Shyi-Long Lee,* and Shiang-Jin Li

Received August 1, 1990

The effects of zero-point energy and counterion on the rate of intramolecular electron transfer in mixed-valence biferrocenium salts are investigated. All asymmetrically substituted biferrocenium triiodide salts, where the substituent is either 1′-ethyl (**9**), 1′-butyl (**10**), 1′-acetyl (**11**), 1′-butyryl (**12**), or 1′-ethyl 6′-propyl (**13**), are found to be localized on the Mössbauer, EPR, and IR time scales. In 300 K Mössbauer spectra they each show two doublets, one for Fe^{II} metallocene and the other for Fe^{III} metallocene (electron-transfer rates less than $\sim 10^7$ s^{-1}). The cation in each of compounds **9**–**13** is not symmetric; that is, the two irons are not in equivalent environments. This asymmetry induces a nonzero zero-point energy barrier for intramolecular electron transfer. The effects on the rate of electron transfer of replacing I_3^- by picrate (**14**), IBr_2^- (**15**), and PF_6^- (**16**) in **2** are also examined. Replacing I_3^- by picrate and IBr_2^- leads to a decrease in the rate of electron transfer. The Mössbauer spectrum taken at 300 K for **14** consists of two doublets. In other words, the electron-transfer rate of **14** is less than $\sim 10^7$ s^{-1}. In the case of **15**, the variable-temperature (100–275 K) Mössbauer spectra exhibit a localized electronic structure. The PF_6^- salt is converted from valence trapped at low temperatures to valence detrapped above 280 K. The difference in electron-transfer rates can be explained by the magnitude of the energy barrier of charge oscillation in anions and cation–anion interactions.

Introduction

Recently, there has been considerable progress made in understanding what factors control the rate of intramolecular electron transfer in the solid state for mixed-valence compounds.[1] In the case of binuclear mixed-valence biferrocenium cations,[2-13] it has been found that the nature of the solid-state environment about a mixed-valence cation can have a dramatic impact on the rate of intramolecular electron transfer. When there is an onset of

Chart I

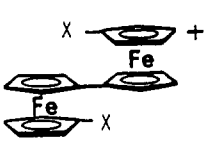

(1) X = -H (5) X = $-CH_2C_6H_5$
(2) X = $-C_2H_5$ (6) X = -I
(3) X = $-C_3H_7$ (7) X = -Br
(4) X = $-C_4H_9$ (8) X = -Cl

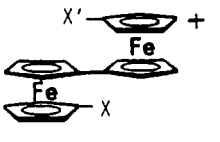

(9) X = -H, X' = $-C_2H_5$
(10) X = -H, X' = $-C_4H_9$
(11) X = -H, X' = -acetyl
(12) X = -H, X' = -butyryl
(13) X = $-C_2H_5$, X' = $-C_3H_7$

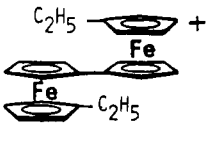

(14) X = -picrate
(15) X = IBr_2
(16) X = $-PF_6$

(1) For recent reviews see: (a) Day, P. *Int. Rev. Phys. Chem.* **1981**, *1*, 149. (b) Brown, D. B., Ed. *Mixed-Valence Compounds, Theory and Applications in Chemistry, Physics, Geology and Biology*; Reidel Publishing Co.: Boston, MA, 1980. (c) Creutz, C. *Prog. Inorg. Chem.* **1983**, *30*, 1–73. (d) Richardson, D. E.; Taube, H. *Coord. Chem. Rev.* **1984**, *60*, 107–129.
(2) Hendrickson, D. N.; Oh, S. M.; Dong, T.-Y.; Kambara, T.; Cohn, M. J.; Moore, M. F. *Comments Inorg. Chem.* **1985**, *4* (6), 329.
(3) Dong, T.-Y.; Cohn, M. J.; Hendrickson, D. N.; Pierpont, C. G. *J. Am. Chem. Soc.* **1985**, *107*, 4777.
(4) Cohn, M. J.; Dong, T.-Y.; Hendrickson, D. N.; Geib, S. J.; Rheingold, A. L. *J. Chem. Soc., Chem. Commun.* **1985**, 1095.
(5) Dong, T.-Y.; Hendrickson, D. N.; Iwai, K.; Cohn, M. J.; Geib, S. J.; Rheingold, A. L.; Sano, H.; Motoyama, I.; Nakashima, S. *J. Am. Chem. Soc.* **1985**, *107*, 7996.
(6) Iijima, S.; Saida, R.; Motoyama, I.; Sano, H. *Bull. Chem. Soc. Jpn.* **1981**, *54*, 1375.
(7) Nakashima, S.; Masuda, Y.; Motoyama, I.; Sano, H. *Bull. Chem. Soc. Jpn.* **1987**, *60*, 1673.
(8) Nakashima, S.; Katada, M.; Motoyama, I.; Sano, H. *Bull. Chem. Soc. Jpn.* **1987**, *60*, 2253.
(9) Dong, T.-Y.; Kambara, T.; Hendrickson, D. N. *J. Am. Chem. Soc.* **1986**, *108*, 4423.
(10) Dong, T.-Y.; Kambara, T.; Hendrickson, D. N. *J. Am. Chem. Soc.* **1986**, *108*, 5857.
(11) Sorai, M.; Nishimori, A.; Hendrickson, D. N.; Dong, T.-Y.; Cohn, M. J. *J. Am. Chem. Soc.* **1987**, *109*, 4266.
(12) Kambara, T.; Hendrickson, D. N.; Dong, T.-Y.; Cohn, M. J. *J. Chem. Phys.* **1987**, *86*, 2326.
(13) Konno, M.; Hyodo, S.; Iijima, S. *Bull. Chem. Soc. Jpn.* **1982**, *55*, 2327.

0020-1669/91/1330-2457$02.50/0

dynamics associated with the counterion, or ligands, this probably will influence the rate of intramolecular electron transfer.[2-9]

Compounds **2–5** (Chart I) give unusual temperature-dependent Mössbauer spectra.[3-6] At temperatures below 200 K they each show two doublets, one for the Fe^{II} and the other for the Fe^{III} site. Increasing the sample temperature in each case causes two doublets to move together with no discernible line broadening, eventually to become a single "average-valence" doublet at temperatures of 275, 245, 275, and 260 K, respectively. Furthermore, pronounced sample history dependence of rates of electron transfer has been noted[5] for compounds **4** and **5**. X-ray structures have been reported at 298 and 140 K for **2**,[14] at 298 and 110 K for **3**,[13] and at 363, 298, and 15 K for **4**.[5] In previous papers,[5,12] we suggested that it is the onset of vibrational motion involving the I_3^- counterion that controls the rate of intramolecular electron transfer in the mixed-valence cation. When the I_3^- counterion is thermally activated, it interconverts between two configurations, $(I_a\cdots I_b-I_c)^-$ and $(I_a-I_b\cdots I_c)^-$. In each of these limiting forms the two iodine–iodine bond lengths are not equal. In effect, the I_3^- counterion is a mixed-valence species itself and the oscillatory charge motion associated with it controls whether charge can be pulled back and forth in the mixed-valence cation.

To increase our sparse knowledge in this area, we have prepared the mixed-valence picrate, PF_6^-, and IBr_2^- salts of **2** in understanding the importance of the counterion in controlling the rate of intramolecular electron transfer in the series of **1–5**. The effects of counterions on intramolecular electron transfer have been reported for **1**,[9] **5**,[15] **6**,[10,16] **7**,[10,16] and **8**.[10] The decrease in electron-transfer rate resulting from replacing I_3^- by IBr_2^- in **6** and **7** was observed.[10] Very recent, Hendrickson reported[15] dramatic changes on electron-transfer rates in **5** as the anion is changed from I_3^- to PF_6^- and SbF_6^-. Sano also found[16] a decrease in electron-transfer rate by replacing I_3^- by $FeCl_4^-$ and $CuBr_2^-$ in **6** and **7**. In this paper, we report the changes in intramolecular electron-transfer rates for the cation of **2** as the anion is changed. Furthermore, the importance of the intrinsic charge-oscillation barrier heights in the mixed-valence cations and anions, as well as the cation–anion interaction, is examined. Results are also presented for the asymmetric mixed-valence biferrocenium complexes (**9–13**). In the PKS vibronic model,[17] it has been assumed that the electronic coupling between the two metal ions, the magnitude of vibronic coupling, and the zero-point energy difference are the most important factors in determining the rate of intramolecular electron transfer. Therefore, it is of interest to see how the zero-point energy difference affects the rate of electron transfer in each of compounds **9–13**. The results of ^{57}Fe Mössbauer, EPR, and IR data are presented in this paper in an attempt to understand the fundamental nature of electron transfer in mixed-valence biferrocenium complexes.

Experimental Section

Compound Preparation. All manipulations involving air-sensitive materials were carried out by using standard Schlenk techniques under an atmosphere of N_2. Chromatography was performed on neutral alumina (activity II), eluting with hexane–CH_2Cl_2. Dichloromethane was dried over P_2O_5. Samples of biferrocene[18] and diethylbiferrocene[6] were prepared according to the literature procedure.

1′-Acylbiferrocenes. The standard method given below is a modification of the procedure of Yamakawa.[19] The acylating reagent was made up according to the Friedel–Crafts synthesis by mixing an equimolar amount of the corresponding acyl chloride and excess $AlCl_3$ in dried CH_2Cl_2 at 0 °C under N_2. The excess $AlCl_3$ was filtered out with glass wool.

The acylating reagent was added by means of a dropping funnel over a period of about 1 h to a solution of biferrocene in dried CH_2Cl_2 at 0 °C. The reaction mixture was stirred from 1 to 3 h at room temperature, and then it was poured into an ice–water mixture. The resulting mixture was separated after the reduction of ferrocenium ion with aqueous sodium thiosulfate. The organic layer was washed with saturated aqueous $NaHCO_3$ and water, and it was then dried over $MgSO_4$. The solvent was removed under reduced pressure. The red oily reside was chromatographed. The crude product was recrystallized from benzene–hexane. In general, the yields are approximately 50%. The synthesized compounds were identified by NMR (Table I) and mass spectral data.

Table I. ^1H NMR Data for Neutral Biferrocenes in $CDCl_3$

compd[a]	chem shift[b]
1′-ethylbifc	4.27 (t, 2 H), 4.22 (s, 2 H), 4.09 (m, 4 H), 3.92 (s, 5 H), 3.82 (s, 4 H), 2.10 (q, 2 H), 0.98 (t, 3 H)
1′-acetylbifc	4.56 (t, 2 H), 4.34 (m, 4 H), 4.30 (t, 2 H), 4.19 (m, 4 H), 3.96 (s, 5 H), 2.13 (s, 3 H)
1′-butylbifc	4.27 (t, 2 H), 4.20 (s, 2 H), 4.10 (t, 2 H), 4.06 (s, 2 H), 3.91 (s, 5 H), 3.80 (m, 4 H), 2.05 (t, 2 H), 1.22 (m, 4 H), 0.79 (t, 3 H)
1′-butyrylbifc	4.49 (t, 2 H), 4.26 (m, 4 H), 4.22 (t, 2 H), 4.12 (m, 4 H), 3.88 (s, 5 H), 2.36 (t, 2 H), 1.53 (m, 2 H), 0.85 (t, 3 H)
1′-ethyl-6′-propylbifc	4.24 (s, 4 H), 4.10 (s, 4 H), 3.84 (s, 8 H), 2.10 (m, 4 H), 1.28 (m, 2 H), 0.98 (t, 3 H), 0.78 (t, 3 H)

[a] bifc is biferrocene. [b] Shifts were taken relative to the TMS peak; d = doublet, t = triplet, q = quartet, and m = multiplet.

Table II. Elemental Analyses for **9–16**

	calcd, %			found, %		
complex	C	H	N	C	H	N
9	33.93	2.85		34.18	2.63	
10	35.73	3.25		36.27	3.08	
11	33.33	2.54		33.13	2.71	
12	35.12	2.95		35.37	2.78	
13	36.58	3.44		36.73	3.20	
14	55.07	4.3	6.42	55.44	4.52	5.56
15	40.44	3.68		40.07	4.02	
16	50.47	4.59		50.63	4.63	

1′-Alkylbiferrocenes. The reduction reaction was carried out by carefully adding, with stirring, small portions of $AlCl_3$ to a mixture of the corresponding acylbiferrocene and $LiAlH_4$ in dried ether. After 30 min, the solution becomes yellow, an excess of H_2O was added to it, and the ether layer was separated. The ether layer was washed with H_2O and dried over $MgSO_4$. After the evaporation of the solvent, the crude product was chromatographed and recrystallized from hexane–benzene in a yield of approximately 90%. Table I lists the ^1H NMR data for the synthesized compounds.

1′-Ethyl-6′-propylbiferrocene. Acetylbiferrocene was propionylated in dried CH_2Cl_2 by following the standard method employed for acylbiferrocene. Chromatography of the crude product that resulted after working up the reaction mixture in the usual manner gave 1′-acetyl-6′-propionylbiferrocene. The title compound was obtained by following the general reduction procedure. The ^1H NMR data are listed in Table I.

Mixed-Valence Compounds. The triiodide and dibromoiodate salts were prepared according to the simple procedure previously reported for the I_3^- and IBr_2^- salts of biferrocenium.[20] Compound **14** was prepared by oxidizing the neutral 1′,6′-diethylbiferrocene dissolved in a minimum amount of benzene by dropwise adding a benzene solution containing a stoichiometric amount of *p*-benzoquinone and picric acid. The dark crude microcrystals were collected by filtration and recrystallized from methanol. The PF_6^- salt **16** was made in a similar manner, dropwise adding a ether solution of HPF_6 and *p*-benzoquinone to a benzene solution of 1′,6′-diethylbiferrocene. The elemental analyses are given in Table II.

Physical Methods. At the Academia Sinica ^{57}Fe Mössbauer measurements were made on a constant-acceleration-type instrument. The source, which originally consisted of 40 mCi of ^{57}Co diffused into a 12-μm rhodium matrix, is connected to a Ranger Scientific Model VT-900 velocity transducer. An Ortec Model 5600 multichannel analyzer, scanned over 1024 channels, receives the logic pulses from the single-channel analyzer. Computer fittings of the ^{57}Fe Mössbauer data to Lorentzian lines were carried out with a modified version of a previ-

(14) Konno, M.; Sano, H. *Bull. Chem. Soc. Jpn.* **1988**, *61*, 1455.
(15) (a) Webb, R. J.; Rheingold, A. L.; Geib, S. J.; Staley, D. L.; Hendrickson, D. N. *Angew. Chem., Int. Ed. Engl.* **1989**, *28*, 1388. (b) Webb, R. J.; Geib, S. J.; Staley, D. L.; Reingold, A. L.; Hendrickson, D. N. *J. Am. Chem. Soc.* **1990**, *112*, 5031.
(16) Kai, M.; Katada, M.; Sano, H. *Chem. Lett.* **1988**, 1523.
(17) Wong, K. Y.; Schatz, P. N. *Prog. Inorg. Chem.* **1981**, *28*, 369.
(18) Rausch, M. D. *J. Org. Chem.* **1961**, *26*, 1802.
(19) Yamakawa, K.; Hisatome, M.; Sako, Y.; Ichida, S. *J. Organomet. Chem.* **1975**, *93*, 219.
(20) Morrison, W. H., Jr.; Hendrickson, D. N. *Inorg. Chem.* **1975**, *14*, 2331.

Table III. ^{57}Fe Mössbauer Least-Squares Fitting Parameters for Asymmetric Mixed-Valence Biferrocenium Salts

complex	ΔE_Q, mm/s	δ,[a] mm/s	Γ,[b] mm/s
9	0.390	0.434	0.280, 0.319
	2.108	0.431	0.253, 0.243
10	0.286	0.448	0.371, 0.436
	2.149	0.428	0.341, 0.340
11	0.484	0.413	0.417, 0.436
	2.037	0.440	0.347, 0.349
12	0.257	0.413	0.292, 0.394
	2.133	0.438	0.257, 0.258
13	0.822	0.430	0.442, 0.420
	1.421	0.440	0.441, 0.469

[a] Isomer shift. [b] Full width at half-height taken from the least-squares fitting program. The width for the line at more positive velocity is listed first for each doublet.

ously reported program.[21] Velocity calibrations were made using a 99.99% pure 10-μm iron foil. Typical line widths for all three pairs of iron lines fell in the range 0.28–0.30 mm/s. Isomer shifts are reported with respect to iron foil at 300 K. It should be noted that the isomer shifts illustrated in the figures are plotted as experimentally obtained; tabulated data should be consulted.

^{1}H NMR spectra were run on a Bruker MSL 200 spectrometer. Mass spectra were obtained with a Hewlett-Packard GC/MS system, Model 5995. Electron paramagnetic resonance data (X-band) were collected with a Bruker ER200D-SRC spectrometer. The magnetic field was calibrated with a Bruker ER035M NMR gauss meter. DPPH was used to gauge the microwave frequency. A direct-immersion dewar, which was inserted into the cavity, was used to obtain 77 K data.

Electrochemical measurements were carried out with a Princeton Applied Research Model 173 instrument. Cyclic voltammetry was performed with a stationary Pt electrode, which was cleaned after each run. Duplicate runs were made on each sample. In most cases the measurements run on 1×10^{-3} M acetonitrile solutions with 0.1 M $(n\text{-}C_4H_9)_4NBF_4$ as supporting electrolyte. Degassing with nitrogen prefaced each run. The potentials quoted in this work are referred to a saturated aqueous calomel electrode at 25 °C.

Theoretical Calculations. Theoretical calculations of charge-oscillation barrier heights in I_3^- and IBr_2^- were performed by using the semi-empirical extended Hückel scheme.[22] In the case of I_3^-, we calculate the potential energy surface for the central iodine atom moving between the two terminal iodines, which were fixed at a distance of 5.85 Å.[5] For the case of IBr_2^-, a similar scheme was performed for the central iodine moving between the two terminal bromine atoms, which were fixed at a distance of 5.404 Å.[23]

Results and Discussion

Physical Properties of Complexes 9–13. The 300 K Mössbauer spectra of **9–13** were obtained, and the absorption peaks were least-squares fitted to Lorentzian lines. The resulting fitting parameters are collected in Table III. The features in the Mössbauer spectra of **9–12** are two doublets, one for iron(II) metallocene ($\Delta E_Q \simeq 2.0$ mm/s) and the other for iron(III) metallocene ($\Delta E_Q \simeq 0.3$ mm/s). This pattern of two doublets is what is expected for a mixed-valence biferrocene that is valence trapped on the time scale of the Mössbauer technique (electron-transfer rate less than $\sim 10^7$ s^{-1}). In the case of compound **13**, the behavior is different from what is seen for **9–12**. The 300 K spectrum for **13** is illustrated in Figure 1. The two doublets, $\Delta E_Q = 0.822$ and 1.421 mm/s, just move together. We believe that the decrease of ΔE_Q in the ferrocenyl doublet and the increase of ΔE_Q in the ferrocenium doublet are related to the degree of intramolecular electron transfer in the mixed-valence biferrocenium cation. In other words, the rate of electron transfer in **13** is the fastest among **9–13**.

The cation in each of compounds **9–13** is not symmetric; that is, the two irons are not in equivalent environments. This asymmetry induces a nonzero zero-point energy barrier for intramolecular electron transfer. One vibronic state of the mixed-valence

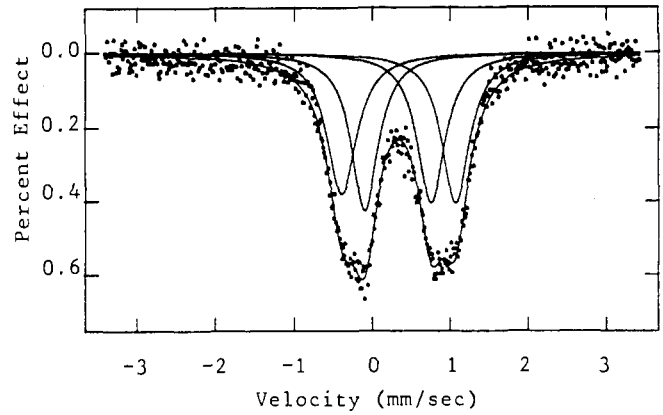

Figure 1. ^{57}Fe Mössbauer spectrum for **13**.

Table IV. Polarographic Data for Various Biferrocenes[a]

compd	$E_{1/2}$, V	Δ,[b] mV	$\Delta E_{1/2}$,[c] V
ferrocene	0.40	65	
bifc[d]	0.31	70	0.32
	0.63	70	
1′,6′-diethylbifc	0.26	65	0.33
	0.59	65	
1′,6′-dipropylbifc	0.25	70	0.33
	0.58	70	
1′-ethylbifc	0.28	70	0.36
	0.64	85	
1′-butylbifc	0.28	75	0.37
	0.65	85	
1′-acetylbifc	0.43	70	0.42
	0.85	85	
1′-butyrylbifc	0.42	70	0.42
	0.84	90	
1′-ethyl-6′-propylbifc	0.26	75	0.33
	0.59	75	

[a] All half-wave potentials are referred to the SCE, employing a stationary Pt electrode. Measurements were run in CH_3CN solution. [b] Peak-to-peak separation between the resolved reduction and oxidation waves maxima. [c] Peak separation between waves. [d] bifc is biferrocene.

cation, i.e., $Fe_a^{II}Fe_b^{III}$, is energetically more stable than the other state, $Fe_a^{III}Fe_b^{II}$. This explains why a localized electronic structure was observed in the series of **9–13**. Furthermore, probably the most important factor controlling the intramolecular electron transfer in a mixed-valence biferrocenium cation is the symmetry of the cation. Complex **13** serves as a very sensitive probe to sense the effect of a nonzero zero-point energy difference on electron transfer. It has been reported that the magnitude of the zero-point energy difference between two vibronic states can be estimated[24] from the two one-electron oxidation waves of unoxidized biferrocene. As shown in Table IV, it can be seen that in each case of asymmetric biferrocene two oxidation waves are detected. From Table IV, the $\Delta E_{1/2}$ values for unoxidized asymmetric biferrocenes, except 1′-ethyl-6′-propylbiferrocene, are larger than that for biferrocene. As reported before, a nonzero zero-point energy difference was induced in the biferrocenium cations **9–12**. In the case of **13**, the zero-point energy difference is not detectable, because the $\Delta E_{1/2}$ values of the 1′,6′-diethyl-, 1′,6′-dipropyl-, and 1′-ethyl-6′-propylbiferrocenes are the same. Complexes **2**[5,6] and **3**[5] are "Mössbauer-delocalized" above 275 and 245 K, respectively. In contrast to complexes **2** and **3**, the cation in **13** has a Mössbauer-localized electronic structure. Hence it appears that the unmeasureable zero-point energy difference plays a rather important role in determining the rate of electron transfer in the mixed-valence cation of **13**. Hendrickson and his co-workers[5] reported the two butyl substituents on the Cp rings in **4** are situated differently, the carbon atom framework of one butyl group parallel to the Cp ring and the other one perpendicular to the Cp ring.

(21) Lee, J. F.; Lee, M. D.; Tseng, P. K. *Hua Hsueh* **1987**, *45*, 50.
(22) Hoffmann, R. *J. Chem. Phys.* **1963**, *39*, 1397.
(23) Williams, J. M.; Wang, H. H.; Beno, M. A.; Emge, T. J.; Sowa, L. M.; Copps, P. T.; Behroozi, F.; Hall, L. N.; Carlson, K. D.; Crabtree, G. W. *Inorg. Chem.* **1984**, *23*, 3841.
(24) Levanda, C.; Bechgaard, K.; Cowan, D. O.; Rausch, M. *J. Am. Chem. Soc.* **1977**, *99*, 2964.

Table V. Electron Paramagnetic Resonance Data[a]

complex	T, K	$g_\parallel$	$g_\perp$	Δg[b]
ferrocenium triiodide[c]	20	4.35	1.26	3.09
1[d]	4.2	3.66	1.73	1.93
2[d]	4.2	3.66	2.01	1.07
			1.89	
4[d]	4.2	2.98	1.92	1.06
9	77	3.35	1.87	1.48
10	77	3.44	1.86	1.58
11[e]	77	2.96	2.00	0.96
12[e]	77	3.38	1.79	1.59
13	77	3.10	1.93	1.17

[a] Powder samples. [b] This is the g-tensor anisotropy defined as $\Delta g = g_\parallel - g_\perp$. [c] See ref 25 and 26. [d] See ref 5. [e] There is some uncertainty in these numbers as a result of broad spectral features.

From our studies, this asymmetry in butyl substituents could play an important role in determining the electron-transfer rate.

The impact of zero-point energy difference could explain why the physical properties of mixed-valence cations **4** and **5** depend on the history of the sample. For example, diffusion-recrystallized **5** gives one average doublet in its 300 K Mössbauer spectrum, whereas the microcrystalline sample gives two doublets at 300 K. In the solid state probably the single most important factor controlling intramolecular electron transfer in a mixed-valence cation experiencing weak or moderate electronic coupling between the two metal centers is symmetry. In the case of the diffusion-recrystallized sample, the environment about a given mixed-valence cation is symmetrical, because the crystallinity is good. In the case of the microcrystalline sample, the possibility of having various kinds of conformational arrangements in the longer alkyl substituents induces a nonzero zero-point energy difference, which leads to a dramatic influence on the rate of intramolecular electron transfer.

X-Band EPR spectra were taken at 77 K for samples of **9–13**. An axial-type spectrum was observed for the five compounds. The g values evaluated from these and other EPR spectra are collected in Table V. Prins reported[27] the g values for a mononuclear ferrocenium cation to be

$$g_\parallel = 2 + 4k[-(\xi/\delta)/(1 + \xi^2/\delta^2)^{1/2}]$$

$$g_\perp = 2/(1 + \xi^2/\delta^2)^{1/2}$$

In these expressions, k is the orbital-reduction factor, ξ is the spin–orbital coupling constant, and δ is a one-electron splitting parameter gauging the effects of crystal fields lower in symmetry than D_5. As the low-symmetry crystal field distortion increases, both $g_\parallel$ and $g_\perp$ approach a value of 2. Hendrickson found[28] that the value of **g** tensor anisotropy (Δ**g**) is considerably reduced for a binuclear mixed-valence biferrocenium cation. Hendrickson suggested that this is a reflection of considerably reduced orbital angular momentum in the ground state that results from admixture of the $S = 0$ Fe^{II} description into the ground state. From Table V, the Δ**g** values for **9–13** are smaller than 1.93 observed[28] for biferrocenium triiodide. This is not a reflection of greater admixture of the $S = 0$ Fe^{II} description into the ground state of iron(III) metallocene. We suggest that the cations in **9–13** would experience a greater low-symmetry crystal field than biferrocenium cation. This could be the origin of the reduced Δ**g** values.

IR spectroscopy has been proven to be useful to tell whether a given mixed-valence biferrocenium cation is delocalized or not.[5,28] When iron(II) metallocene is oxidized to iron(III) metallocene, there is a dramatic change in the IR spectrum. It has been shown[29] that the perpendicular C–H bending band is the best diagnosis of the oxidation state. This band is seen at 815 cm^{-1} for ferrocene and at 850 cm^{-1} for ferrocenium triiodide. Mixed-valence biferrocenium cations that have a nonnegligible potential energy barrier for electron transfer should exhibit one C–H bending band for the Fe^{II} moiety and one for the Fe^{III} moiety. IR spectroscopy has been employed to study mixed-valence complexes **9–13**. The perpendicular C–H bending modes for **9–13** are given in Table

Table VI. IR Data for the C–H Bending Mode

	C–H bending mode			C–H bending mode	
complex[a]	Fe(II)	Fe(III)	complex[a]	Fe(II)	Fe(III)
1′-ethylbifc	810		**11**	822	845
9	820	832	1′-butyrylbifc	818	
1′-butylbifc	810		**12**	827	841
10	820	835	**13**	815	830
1′-acetylbifc	811				

[a] bifc is biferrocene.

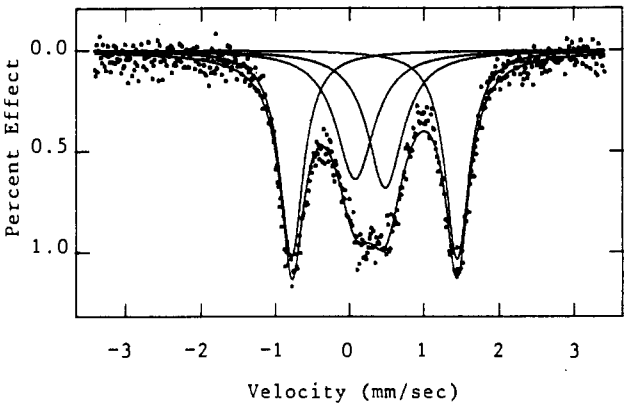

Figure 2. ^{57}Fe Mössbauer spectrum for **14**.

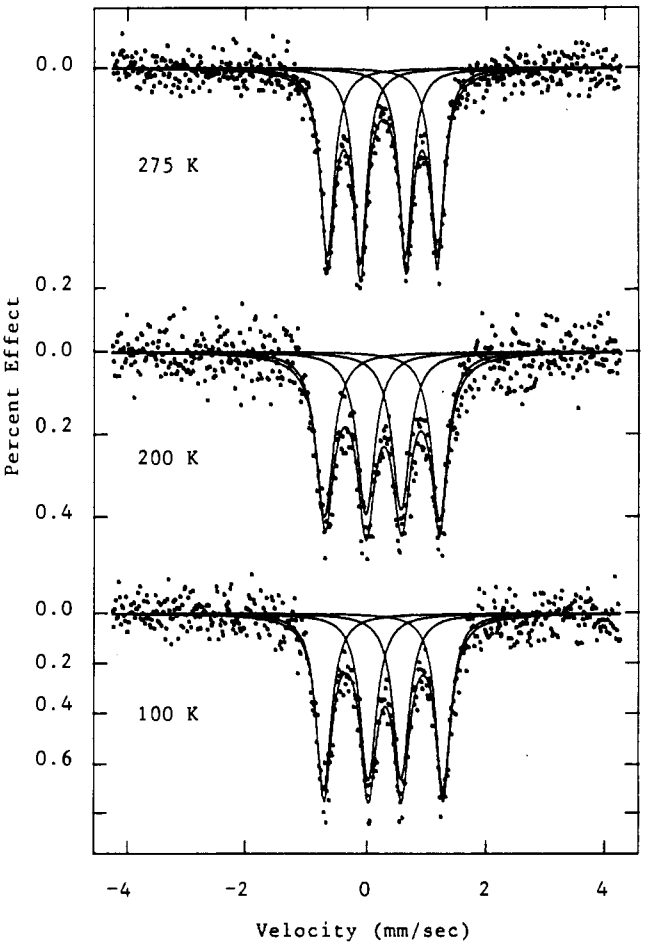

Figure 3. Variable-temperature ^{57}Fe Mössbauer spectrum for **15**.

(25) Sahn, Y. S.; Hendrickson, D. N.; Gray, H. B. *J. Am. Chem. Soc.* **1971**, *93*, 3603.
(26) Duggan, D. M.; Hendrickson, D. N. *Inorg. Chem.* **1975**, *14*, 955.
(27) Prins, R.; Kortberk, A. *J. Organomet. Chem.* **1971**, *33*, C33.
(28) Dong, T.-Y.; Hendrickson, D. N.; Pierpont, C. G.; Moore, M. F. *J. Am. Chem. Soc.* **1986**, *108*, 963.
(29) Kramer, J. A.; Hendrickson, D. N. *Inorg. Chem.* **1980**, *19*, 3330.

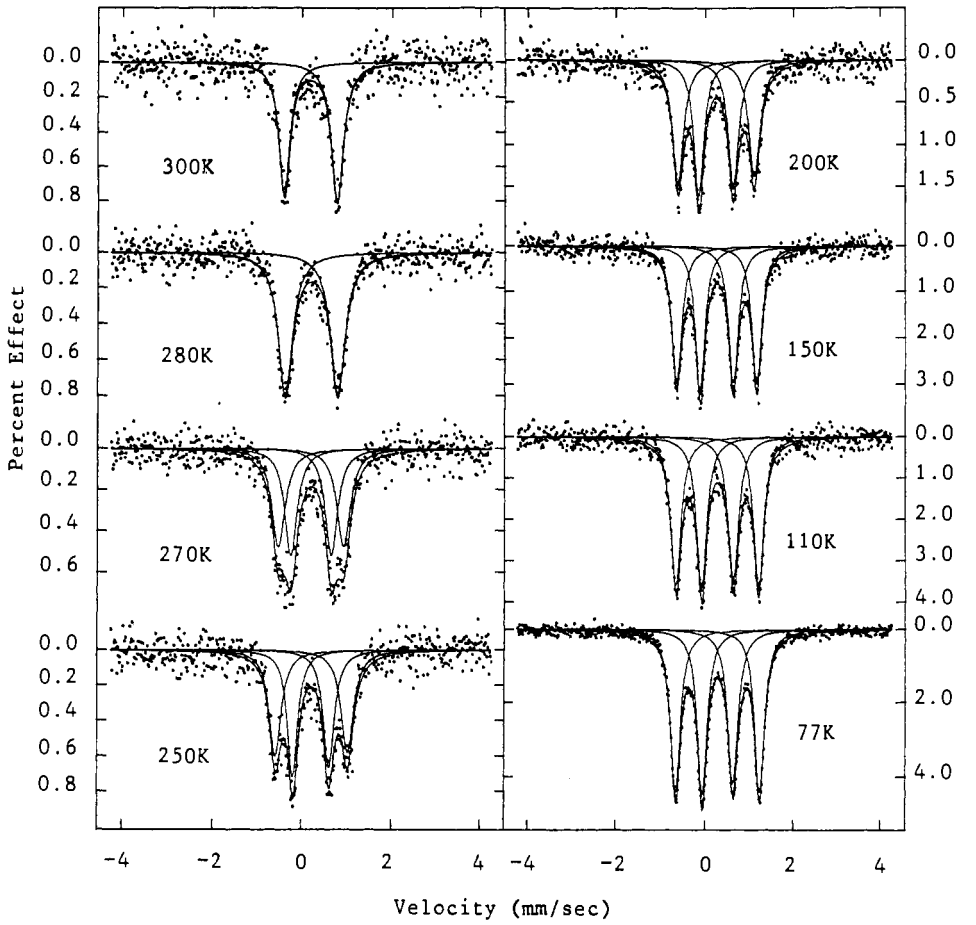

Figure 4. Variable-temperature Mössbauer spectrum for **16**.

VI. It is clear that the IR data for **9–13** conclusively indicate the presence of Fe^{II} and Fe^{III} moieties.

Counterion Effect on the Electron Transfer. The replacements of the I_3^- anion of **2** by picrate, IBr_2^-, and PF_6^- exhibit interesting Mössbauer characteristics. A Mössbauer spectrum taken at 300 K for a microcrystalline sample of **14** is shown in Figure 2. This spectrum was least-squares fitted to Lorentzian line shapes, and the fitting parameters are given in Table VII. The spectrum consists two quadrupole-split doublets, one characteristic of an iron(II) metallocene with a quadrupole splitting of ΔE_Q = 2.2049 mm/s and other characteristic of an iron(III) metallocene with ΔE_Q = 0.4043 mm/s. This pattern of two doublets is what is expected for a mixed-valence biferrocene that is valence trapped on the time scale of the ^{57}Fe Mössbauer experiment. Thus, the change from I_3^- in **2** to picrate anion in **14** leads to a dramatic reduction of intramolecular electron-transfer rate. This change clearly indicates that the solid-state environment about a given mixed-valence cation plays a crucial role in determining the rate of intramolecular electron transfer.

In Figure 3 are shown variable-temperature Mössbauer spectra for a microcrystalline sample of **15**. A comparison of the Mössbauer data reported for **2** with those for **15** indicates that these two compounds have similar Mössbauer temperature dependence; however, everything is shifted to higher temperatures for the IBr_2^- salt. As is evident in Table VII, the ΔE_Q value for the Fe^{III} signal gradually increases and the ΔE_Q value for the Fe^{II} signal gradually decreases. In the case of **2**, the variable-temperature Mössbauer spectra exhibit a delocalized electronic structure above 275 K.[5] However, a much higher range of temperature is needed for the complete conversion from localized to delocalized for **15**. Unfortunately, the IBr_2^- salt **15** decomposes at temperatures above 290 K. In our previous paper,[10] the decrease in electron-transfer rate resulting from replacing I_3^- by IBr_2^- in **6** and **7** was also observed. Furthermore, we found the opposite effect on the electron-transfer rate by replacing the I_3^- anion for **1** by IBr_2^-.[9] An explanation for this difference is presented in the last section, which keys on the different packing arrangements in the mixed-valence compounds.

Table VII. ^{57}Fe Mössbauer Least-Squares Fitting Parameters for **14–16**

complex	T, K	ΔE_Q, mm/s	δ,[a] mm/s	Γ,[b] mm/s
14	300	0.4043	0.3870	0.5786, 0.6166
		2.2049	0.4384	0.3774, 0.3831
15	100	0.5420	0.3999	0.3195, 0.3171
		1.9603	0.3922	0.2999, 0.2994
	200	0.5777	0.3760	0.3514, 0.3411
		1.8801	0.3640	0.3282, 0.3361
	275	0.7429	0.3677	0.2702, 0.2597
		1.8024	0.3689	0.2723, 0.2687
16	77	0.6936	0.3877	0.2838, 0.2655
		1.8858	0.3888	0.2693, 0.2690
	110	0.7166	0.3804	0.2912, 0.2764
		1.8537	0.3805	0.2777, 0.2793
	150	0.7409	0.3642	0.2719, 0.2580
		1.8021	0.3697	0.2691, 0.2752
	200	0.7685	0.3335	0.2880, 0.2662
		1.7212	0.3396	0.3127, 0.2946
	250	0.7893	0.3235	0.2979, 0.2754
		1.6015	0.3324	0.3409, 0.3297
	270	0.8973	0.3060	0.3468, 0.3468
		1.4234	0.3034	0.3667, 0.3667
	280	1.1565	0.3188	0.3990, 0.3829
	300	1.1666	0.3005	0.3254, 0.2991

[a] Isomer shift. [b] Full width at half-height taken from the least-squares fitting program. The width for the line at more positive velocity is listed first for each doublet.

Mössbauer spectra were run at temperatures in the range 77–300 K for the PF_6^- salt **16**. These spectra are shown in Figure 4; fitting parameters are collected in Table VII. As shown in Figure 4, complex **16** is converting from valence trapped at low temperature to valence detrapped above 280 K. That is, at low temperatures there are two doublets, one characteristic of an Fe^{II}

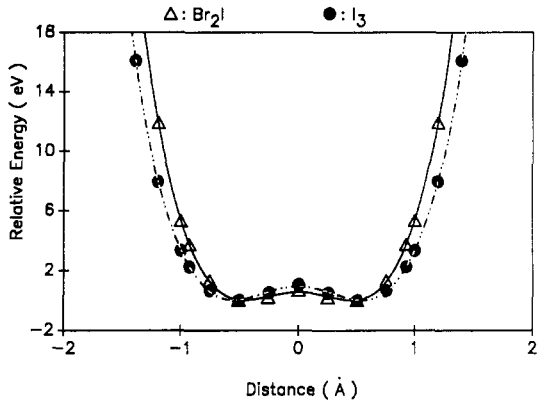

Figure 5. Charge-oscillation barrier heights in I_3^- and IBr_2^-.

site and the other characteristic of an Fe^{III} site. As the temperature is increased, the two doublets move together with no line broadening to become a single doublet above 280 K. If the intramolecular electron transfer in **16** was slower than the Mössbauer time scale (rate $< \simeq 10^7\ s^{-1}$) at low temperature and then increased with increasing temperatures, the line widths of each doublet would be expected to broaden as the electron-transfer rate goes through the ^{57}Fe Mössbauer window. Absence of line broadening in Mössbauer spectra has been noted for **2-5**.[5] It has been concluded that the process which leads to the averaging seen in Mössbauer studies occurs at a rate faster than the Mössbauer time scale at all temperatures.

Micromodulation of Rate of Intramolecular Electron Transfer. The goal of this section is to present an explanation for the pronounced influence that the anion has on the rate of intramolecular electron transfer in mixed-valence biferrocenium salts. In Hendrickson's theoretical model,[12] the factors that are potentially important in controlling the rate of intramolecular electron transfer in the mixed-valence biferrocenium cation include (1) the effective barrier for electron transfer in the cation, (2) the effective barrier for charge oscillation in the anion, and (3) the intermolecular cation-cation and cation-anion interactions. In general, it has been suggested that the greater the effective barrier for charge oscillation in the cation or anion, the smaller the electron-transfer rate. Furthermore, the electron-transfer rate will be decreased with increasing cation-anion interaction.

Possible origins of the effect of replacing I_3^- by IBr_2^- in mixed-valence biferrocenium salts can now be proposed. From the theoretical calculations (Figure 5), the IBr_2^- anion could have a smaller barrier for charge oscillation than does the I_3^- anion. This would explain why the mixed-valence biferrocenium dibromoiodide has an electron-transfer rate in excess of $10^7\ s^{-1}$ at a temperature 150 °C lower than that observed for biferrocenium triiodide.

Replacing I_3^- by IBr_2^- for mixed-valence 1',6'-diethyl- and 1',6'-diiodobiferrocenium cations has the opposite effect; the rate of electron transfer is reduced at a given temperature. The X-ray structure of **6**[28] reveals that in each stack of anions and cations there is an appreciable interaction between the terminal atoms of the I_3^- anions and the iodine atom on the Cp ring of the cation. Thus, there is a larger in-stack cation-anion interaction in the IBr_2^- salt than in the I_3^- salt. The increased cation-anion interaction in the IBr_2^- salt effectively reduces the rate of intramolecular electron transfer. The same could be happening in **15**. In fact, from the X-ray structure of **2**, Sano reported that there is a significant cation-anion interaction (3.78 Å) in this compound. Because the terminal bromine atoms in IBr_2^- carry more net negative charge than the terminal iodine atoms of I_3^-, the interaction between the terminal bromine and cation would be greater than the analogous interaction in the I_3^- salt. The increased cation-anion interaction in the IBr_2^- salt **15** also reduces the rate of electron transfer.

Conclusion

In this paper, we demonstrate that relatively minor perturbations caused by interactions with neighboring cations and anions in biferrocenium salts experiencing weak or moderate electronic coupling between two Fe centers have pronounced effects on the electronic structure and rate of intramolecular electron transfer. Furthermore, the influence of the nonzero zero-point energy difference on the rate of intramolecular electron transfer appears to be quite pronounced in compounds **9-13**.

Acknowledgment. We are grateful for support from the National Science Council (TYD).

Contribution from the Department of Chemistry, College of Arts and Sciences, The University of Tokyo, 3-8-1 Komaba, Meguro-ku, Tokyo 153, Japan

X-ray Diffraction and Electric Dichroism Studies on the Adsorption of Metal Complexes by a Clay

Masahiro Taniguchi, Akihiko Yamagishi,* and Toschitake Iwamoto

Received October 16, 1989

The binding structures of enantiomeric and racemic $[M(phen)_3]^{2+}$ (M = Ru, Fe; phen = 1,10-phenanthroline) complexes with sodium montmorillonite were studied by means of X-ray diffraction and electric dichroism measurements. The electron density curves along the *c* axis of a clay layer were determined for the powder samples of clay-chelate adducts. At maximum adsorption, the enantiomeric and racemic chelates formed the single-molecular and double-molecular layers in the interlayer spaces, respectively. The reduced linear dichroisms for the two characteristic bands in their electronic absorption spectra (i.e. the metal-to-ligand charge-transfer band at 400-500 nm and the ligand excitation bands at 240-280 nm) were determined for the bound metal complexes in a colloidal state. The orientation of a bound complex was elucidated by comparing the observed reduced linear dichroism with the ones calculated for the possible bound state in the interlayer space of a clay. The chelate was bound to a clay with its 3-fold symmetry axis at an angle of 60-65° with respect to the surface. No difference was observed for the orientations of the bound species between the racemic mixture and the pure enantiomer of the complex.

Introduction

We have been studying the adsorption of a metal complex by a clay, focusing our attention on the stereochemical effects on its bound states.[1,2] Metal complexes studied so far possess bulky planar ligands such as $[M(phen)_3]^{2+}$ and $[M(PAN)_3]^+$ (phen = 1,10-phenanthroline, and PAN = (1-pyridine-2-azo)-2-naphthol). It is found that the maximum adsorption amount is different when a metal complex is added as either a racemic mixture or a pure

* To whom correspondence should be addressed.

(1) Yamagishi, A.; Soma, M. *J. Am. Chem. Soc.* **1981**, *103*, 4640.
(2) Yamagishi, A. *J. Coord. Chem.* **1987**, *16*, 131.

0020-1669/91/1330-2462$02.50/0